Phys. Lett. B 868 (2025) 139815

Contents lists available at ScienceDirect

Physics Letters B

journal homepage: www.elsevier.com/locate/physletb

Letter

Constraining the nuclear symmetry energy with Fermi-energy heavy ion collisions

C. Ciampi [a,*], S. Mallik [b,c], F. Gulminelli [d], D. Gruyer [d], J. D. Frankland [a], N. Le Neindre [d], R. Bougault [d], A. Chbihi [a], L. Baldesi [e,f], S. Barlini [e,f], B. Borderie [g], A. Camaiani [e,f], G. Casini [e], I. Dekhissi [d], J. A. Dueñas [h], Q. Fable [a], F. Gramegna [i], M. Henri [j], B. Hong [k,l], S. Kim [m], A. Kordyasz [n], T. Kozik [o], I. Lombardo [p,q], O. Lopez [d], T. Marchi [i], S. H. Nam [k,l], J. Park [k,l], M. Pârlog [d,r], G. Pasquali [e,f], S. Piantelli [e], G. Poggi [e,f], S. Valdré [e], G. Verde [p,s], E. Vient [d]

[a] Grand Accélérateur National d'Ions Lourds (GANIL), CEA/DRF-CNRS/IN2P3, Boulevard Henri Becquerel, F-14076, Caen, France
[b] Physics Group, Variable Energy Cyclotron Centre, 1/AF Bidhan Nagar, 700064, Kolkata, India
[c] Homi Bhabha National Institute, Training School Complex, Anushakti Nagar, 400085, Mumbai, India
[d] Université de Caen Normandie, ENSICAEN, CNRS/IN2P3, LPC Caen UMR6534, F-14000, Caen, France
[e] INFN - Sezione di Firenze, 50019, Sesto Fiorentino, Italy
[f] Dipartimento di Fisica e Astronomia, Università di Firenze, 50019, Sesto Fiorentino, Italy
[g] Université Paris-Saclay, CNRS/IN2P3, IJCLab, 91405, Orsay, France
[h] Departamento de Ingeniería Eléctrica y Centro de Estudios Avanzados en Física, Matemáticas y Computación, Universidad de Huelva, 21007, Huelva, Spain
[i] INFN - Laboratori Nazionali di Legnaro, 35020, Legnaro, Italy
[j] CEA/INSTN/UECC, 143 Chemin de la Crespinière - ZA Les Vindits, F-50130, Cherbourg en Cotentin, France
[k] Center for Extreme Nuclear Matters (CENuM), Korea University, 02841, Seoul, Republic of Korea
[l] Department of Physics, Korea University, 02841, Seoul, Republic of Korea
[m] Center for Exotic Nuclear Studies, Institute for Basic Science, 34126, Daejeon, Republic of Korea
[n] Heavy Ion Laboratory, University of Warsaw, 02-093, Warszawa, Poland
[o] Marian Smoluchowski Institute of Physics Jagiellonian University, 30-348, Krakow, Poland
[p] INFN - Sezione di Catania, 95123, Catania, Italy
[q] Dipartimento di Fisica e Astronomia, Università di Catania, via S. Sofia 64, 95123, Catania, Italy
[r] "Horia Hulubei" National Institute for R&D in Physics and Nuclear Engineering (IFIN-HH), P. O. Box MG-6, Bucharest Magurele, Romania
[s] Laboratoire des 2 Infinis - Toulouse (L2IT-IN2P3), Université de Toulouse CNRS, UPS, F-31062 Toulouse Cedex 9, France

ARTICLE INFO

Editor: Prof. Betram Blank

Keywords:
Nuclear equation of state
Symmetry energy
Isospin transport
Isospin diffusion

ABSTRACT

Heavy ion reactions provide a unique opportunity to unveil the Equation of State (EoS) of baryonic matter in a large density domain. However, to get quantitative constraints it is crucial to employ observables that are as insensitive as possible to final state interaction, and at the same time robustly predicted by transport models with limited model dependence. In this work, we compare for the first time BUU transport calculations to the impact parameter dependence of the isospin transport ratio deduced from INDRA-FAZIA data [1], with a model independent evaluation of the impact parameter. Using different state-of-the-art nuclear functionals, provided both by fits of *ab initio* calculations and by phenomenological approaches, a confidence region for the symmetry energy is extracted. A consistent study of the time dependence of the baryonic density and of the isospin current density allows a precise determination of the density region significantly probed by the experiment, with the definition of confidence regions in the symmetry energy *vs* density plane. A symmetry energy $S = (29.0 \pm 0.7)$ MeV is obtained for the most significant density $\rho/\rho_0 = 1.01$. The obtained symmetry energy constraint can be used to inform Bayesian inference of the neutron star EoS.

1. Introduction

Heavy-ion collisions (HIC) are unique probes to explore in the laboratory nuclear matter in density conditions different from the one of atomic nuclei at ground state, and can thus potentially bring important constraints to the nuclear Equation of State (EoS) [2], an essential ingredient to the interpretation of gravitational wave data [3]. This is particularly true in the (ultra-) relativistic regime [4], where collective

* Corresponding author.
E-mail addresses: caterina.ciampi@ganil.fr (C. Ciampi), swagato@vecc.gov.in (S. Mallik).

https://doi.org/10.1016/j.physletb.2025.139815
Received 14 March 2025; Received in revised form 18 June 2025; Accepted 8 August 2025
Available online 10 August 2025

flows and particle production can be compared with transport model calculations in controlled numerical settings [5,6] to extract the density dependence of the symmetry energy [7] in a density domain lying between the one explored by *ab initio* calculations [8] and nuclear structure experiments [9,10], and the one probed by astrophysical measurements [11]. Still, the HIC intermediate energy domain provides complementary observables that can meaningfully enrich the available constraints, with the additional advantage that the momentum dependence can still be controlled by the effective mass formalism, and uncertainties on the elementary reaction rates are strongly reduced.

In particular, in Fermi energy HIC, the differential transfer of protons and neutrons between projectile and target, called isospin diffusion, can be measured by the Isospin Transport Ratio (ITR), defined as [12]:

$$R_i(x) = \frac{2x_i - x_{(A+A)} - x_{(B+B)}}{x_{(A+A)} - x_{(B+B)}}. \quad (1)$$

Here x is an isospin sensitive observable extracted from the final state of reactions between two nuclides A and B, with different neutron-richness, with $i = (A+B), (B+A)$. The value x_i measured for reactions between nuclei with different neutron content is normalized to the reference values obtained when the same nuclide is used for both projectile and target, $(A+A)$ and $(B+B)$. The pioneering works of the MSU group [13] showed that the ITR is strongly correlated to the density dependence of the symmetry energy, allowing the exclusion of extreme values for its magnitude and slope around saturation density ($E_{\rm sym}$ and $L_{\rm sym}$ parameters) [14]. However, to get quantitative constraints, different delicate points need to be addressed: (1) the isospin sensitive observable must be chosen such that it is directly measurable and at the same time robustly predicted by the transport model [15]; (2) the reaction centrality assessment must be reliable and readily comparable between model and data; (3) the density range probed by the ITR in the studied reactions must be estimated to avoid uncontrolled extrapolations. In particular, a huge number of works have extracted constraints on both $E_{\rm sym}$ and $L_{\rm sym}$ from the optimization of effective EoS models to the reproduction of isospin sensitive observables in the sub-saturation regime [16–18]. However, the density probed by the different experiments should be estimated to settle the effect of a possible extrapolation to these saturation density quantities, and the density domain where these constraints can be applied.

In this work, we propose significative improvements to all these points. First, the ITR is evaluated using the directly measured neutron to proton ratio of the quasiprojectile remnant [1,19], a particularly robust observable for the transport models, providing an ITR with very limited sensitivity to secondary decay [20,21]. This key improvement was possible due to the excellent isotopic identification performance of the FAZIA apparatus [22,23], able to achieve mass discrimination for heavy nuclei up to $Z \approx 25$. Second, for the centrality assessment we employ a model-independent method to reconstruct the impact parameter distributions contributing to each data point [24]. Finally, for the model comparison we employ a twofold strategy. On one side, we include in our functional choice two models fitted from *ab initio* calculations, that explore the present uncertainty of chiral-EFT (χ-EFT) predictions [25]; moreover, to understand which part of the functional can be effectively probed by the comparison, we estimate precisely the density associated to the isospin transfer by correlating the time evolution of the isospin current densities [26] and the nuclear density.

2. Experimental data and theoretical predictions

2.1. INDRA-FAZIA experimental data

We consider ^{58,64}Ni + ^{58,64}Ni reactions at 32 MeV/nucleon measured with the INDRA-FAZIA apparatus at GANIL: this dataset has been employed also in Refs. [19,27], where further experimental details can be found. The experimental data was analyzed [1] with the aim of producing the most model-independent results possible in order to facilitate comparison with the predictions of any transport model. The isospin sensitive observable used to compute the ITR is the average neutron-to-proton ratio $\langle N/Z \rangle$ of the quasiprojectile remnant, identified event-by-event as the forward-emitted fragment with the largest atomic number. The experimental result for the ITR $R(\langle N/Z \rangle)$ as a function of the impact

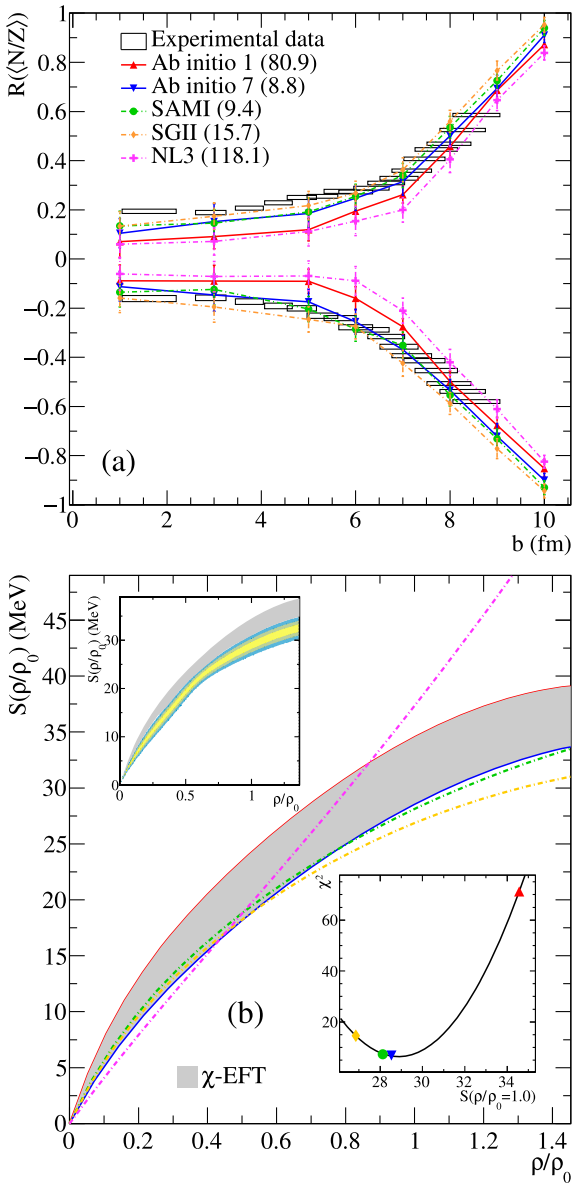

Fig. 1. Impact parameter dependence of the isospin transport ratio R obtained from the $\langle N/Z \rangle$ of quasiprojectile for ^{64}Ni + ^{58}Ni and ^{58}Ni + ^{64}Ni reactions at 32 MeV/nucleon (a). The experimental results from Ref. [1], shown as open rectangles delimiting the uncertainties, are compared with BUU@VECC-McGill model calculations adopting *ab initio* 1, *ab initio* 7, SAMI, SGII and NL3 EoS parametrizations (lines are drawn to guide the eyes): the corresponding χ^2-values are indicated in parentheses in the legend. The symmetry energy density dependence for the five EoS hereby tested is plotted in (b) using the same color and line-type scheme. Dash-dotted (solid) lines indicate phenomenological (*ab initio*) models. The gray band indicates the uncertainty on the microscopic constraint from χ-EFT. The bottom-right inset in (b) shows with a black line the quadratic fit of $\chi^2(S(\rho/\rho_0))$ for $\rho/\rho_0 = 1$, as an example of the procedure. The top-left inset in (b) shows the posterior distribution of $S(\rho/\rho_0)$ without applying to the flat prior the weight $p_i^{prior} = w(\rho_i/\rho_0)$ described in Section 3.

parameter b is plotted in Fig. 1(a) with open rectangles [1] representing statistical errors on the y-axis, and the combined effect of statistical errors with those associated with the uncertainties in the b reconstruction procedure [24] along the x-axis. As done in Ref. [1], in Fig. 1(a) the experimental points for more peripheral collisions have been already excluded, since they can be affected by the limitation of the apparatus in terms of mass identification.

2.2. Model calculations

The theoretical calculations are performed using the BUU@VECC-McGill transport model [28,29], shown to produce results consistent with similar models in the systematic survey conducted by the Transport Model Evaluation Project (TMEP) [5], both for mean-field [30] and nucleon-nucleon collisions [31]. Ground states of the projectile and target nuclei are constructed with a variational method [32] using Myers density profiles [33]. We use 100 test particles per nucleon. For each reaction, the calculation is carried out for eight impact parameter settings up to the grazing value; for each one of them, 200 events are simulated, due to the long computation time required. The bulk part of the mean-field is calculated from a meta-functional [34] based on a polynomial expansion in density around saturation and including momentum dependence and deviations from the parabolic isospin dependence through the effective mass and its splitting. To cover the present uncertainty on the density dependence of the symmetry energy at sub-saturation, the EoS from two χ-EFT interactions leading to extreme behaviors in pure neutron matter (PNM) (specifically models 1 and 7 in Ref. [25], here abbreviated as *ab initio* 1 and *ab initio* 7, respectively), are considered. The density dependence of the symmetry energy from these two EoS is presented in Fig. 1(b) with solid lines. The gray band of Fig. 1(b) thus indicates the present uncertainty on the density dependence of the symmetry energy from these nuclear matter *ab initio* calculations [25]. If χ-EFT provides to date the most accurate predictions for low density PNM, it suffers considerable uncertainties in the isoscalar channel and above saturation density ρ_0. For this reason, we also consider two popular effective models, the relativistic mean-field NL3 [35] and the SGII Skyrme interaction [36], that respect the PNM χ-EFT constraint at low density but correspond to a stiff (respectively, soft) extrapolation for supra-saturation matter. Such relatively extreme behaviors were suggested by analyses of neutron skin measurements [37] and pion production data [38], respectively. The symmetry energy density dependence corresponding to these phenomenological approaches is plotted in Fig. 1(b) with dash-dotted lines. Finally, the Skyrme interaction SAMI [39] is also considered, that corresponds to a symmetry energy behavior almost indistinguishable from *ab initio* 7 but a more realistic behavior for symmetric matter. The comparison between these two models, SAMI and *ab initio* 7, will therefore allow to verify that the adopted observable is indeed suitable to explore isovector properties and is not sensitive to isoscalar ones. For treating finite nuclei, the bulk part is supplemented by a finite range term optimized on nuclear masses [40] as well as Coulomb potential. For more details, we refer the reader to [41].

The ITR predicted by the BUU@VECC-McGill calculations assuming the aforementioned interaction models are displayed in Fig. 1(a), where the same color and line-type scheme as in Fig. 1(b) is employed. In each case, the calculations are run until convergence of the ITR (see Ref. [20]), calculated with the $\langle N/Z \rangle$ of the primary quasiprojectile without secondary de-excitation, thus avoiding possible spurious effects arising from coupling the transport model with an afterburner. Consequently, no experimental filter is applied to the simulations. The model error bars represent statistical errors due to the finite number of events. The different models here employed fall within the relatively tight limits for the symmetry energy estimated from present constraints (see Fig. 1(b)) and therefore produce similar ITR values, with a similar impact parameter dependence. In particular, we note that the excellent agreement between the *ab initio* 7 and the SAMI results shows that the ITR is indeed probing the density dependence of the symmetry energy.

2.3. Discussion

Fig. 1(a) also allows to compare the experimental ITR to those predicted by the BUU code: for reference, χ^2 values resulting from the comparison between experimental data and model predictions for the different EoS here considered are reported in parentheses in the legend. It should be noted that such a comparison is possible thanks to the fact that the ITR strongly suppresses systematic effects in the data such as secondary decay and experimental acceptance [20,21]. Even if the differences among the theoretical predictions are small, we can still see that the models with the highest symmetry energy around saturation, namely *ab initio* 1 and NL3, can be excluded, in agreement with previous works [16]. The most satisfying match of the ITR with the experimental data is provided by SAMI, SGII and *ab initio* 7, all characterized by similar symmetry energy values in this density region. To quantify the quality of the agreement of a given model m with the data we use the quantity $\chi^2_m = \sum_{b=b_{\min}}^{b_{\max}} (R(b) - R^{(m)}(b))^2 / 2\sigma^2_m(b)$, where the sum runs over impact parameters, $R^{(m)}(b)$ is the theoretical prediction for the ITR within model m, and $\sigma^2_m = \sigma^2_{exp}(b) + \sigma^2_{th,m}(b)$ accounts for both experimental and theoretical uncertainties. Here, we consider impact parameters between $b_{\min} = 3$ fm and $b_{\max} = 9$ fm, where most of the information from the experimental data is concentrated.

The extracted χ^2_m values for the parametrizations under test can be employed to provide approximate confidence regions in the $S - \rho/\rho_0$ plane. To do this, for each ρ_i bin, the posterior distribution of $S_i \equiv S(\rho_i)$ can be expressed as:

$$p_i(S_i|ITR) = \mathcal{N} \sum_m p_i(m|ITR)\, \delta\big(S_i - S^{(m)}(\rho_i)\big), \tag{2}$$

where the sum runs over models, $S^{(m)}(\rho_i)$ is the value of S at density ρ_i corresponding to the model m, and $\mathcal{N}$ is a normalization; the model posterior distribution $p_i(m|ITR)$ is given by Bayes theorem using a gaussian likelihood:

$$p_i(m|ITR) = p_i^{prior} \exp(-\chi^2_m/2), \tag{3}$$

where in each density bin we consider a flat prior for S, $p_i^{prior} = w(\rho_i/\rho_0)$, and the different bins are weighted with a function that measures the density probed by the experiment, as described in the next section. In principle, the χ^2 value should be calculated on a large set of models covering the symmetry energy prior, which is a formidable computational task. However, in a large range of densities $0.4 \lesssim \rho/\rho_0 \lesssim 1.1$ a parabolic dependence of χ^2_m is observed when this latter is plotted as a function of $S(\rho/\rho_0^{(m)})$. Therefore, as a first step towards a complete Bayesian exploration of the parameter space, we interpolate the likelihood of symmetry energy values that lie between the ones explored by the chosen models, with a quadratic fit[1]. The inset of Fig. 1(b) provides an example of the fit for $\rho/\rho_0 = 1$.

3. Determination of the probed baryonic densities

The process of isospin diffusion probes the different densities explored by the system with varying sensitivity, which must be accounted for in view of providing a constraint on the symmetry energy density dependence. To this end, further information on the dynamics of this process can be extracted from the BUU@VECC-McGill transport model calculations, in order to define a weight function $w(\rho/\rho_0)$ quantifying the ITR sensitive region, defined as the density interval explored in the dynamical evolution during the process of isospin transfer.

We therefore focus on the baryonic density and on the isospin current density. Their time evolution has been extracted and averaged over $N_{ev} = 200$ events for four different impact parameter settings, namely $b = 3$, 5, 7 and 9 fm, assuming an *ab initio* 7 EoS (similar behaviors

[1] The result for NL3, giving the worst agreement with the experimental data, has been excluded from the fit procedure.

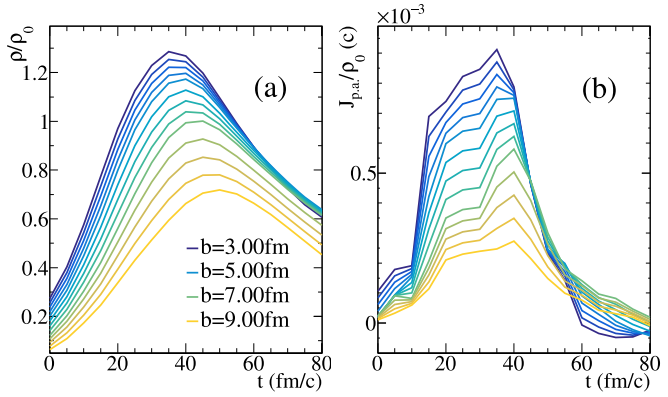

Fig. 2. Time dependence of (a) the baryonic density ρ/ρ_0, (b) the component of the isospin current density along the principal axis $j_{\text{p.a.}}/\rho_0$ for ^{64}Ni+^{58}Ni at 32 MeV/nucleon at different impact parameters between $b=$ 3 fm and 9 fm, obtained from BUU@VECC-McGill calculations with *ab initio* 7 EoS.

are obtained for the SAMI EoS). The behavior for intermediate impact parameters has been obtained through interpolation. At each timestep, the baryonic density is calculated within a spherical volume V of radius $r = 3$ fm around the origin of the center of mass frame (see Appendix A for more details); its time evolution is shown in Fig. 2(a) for ^{64}Ni+^{58}Ni at 32 MeV/nucleon for a few impact parameters. The isospin current density is defined as $\vec{j}_I = \Delta\vec{j}_n - \Delta\vec{j}_p$, where $\Delta\vec{j}_q = \vec{j}_q^{(P)} + \vec{j}_q^{(T)}$ is the net current density associated to species $q = n, p$ leading to particle exchange from the two colliding nuclei, with:

$$\vec{j}_q^{(X)} = \frac{1}{V}\int_V d^3r \rho_q^{(X)}(\vec{r})\vec{v}_q^{(X)}(\vec{r}). \tag{4}$$

where the local current density is averaged over the same spherical volume V of radius $r = 3$ fm employed for the baryonic density estimation. Here, the local particle density $\rho_q^{(X)}$ and velocity $\vec{v}_q^{(X)}$ is calculated by considering separately the test particles belonging to the projectile (P) and target (T) nucleus before the collision. To follow the dynamics of isospin transfer, the local velocity $v_q^{(X)}$ and isospin current density $\vec{j}_q^{(X)}$ must be calculated along the time-dependent principal axis (p.a.), obtained by diagonalizing at each time step the events averaged momentum of inertia tensor:

$$I_{xx} = \sum_{i=1}^{N_{tot}} m\left(y_i^2 + z_i^2\right) \; ; \; I_{zz} = \sum_{i=1}^{N_{tot}} m\left(y_i^2 + x_i^2\right) \; ; \tag{5}$$

$$I_{xz} = -\sum_{i=1}^{N_{tot}} m x_i z_i \; , \tag{6}$$

where m is the nucleon mass, the sum runs over the test particles and (x, z) is the reaction plane. The component of the isospin current density along the principal axis $j_{\text{p.a.}}$ is the one contributing to the nucleon exchange between the two colliding nuclei: its time evolution for a few impact parameters is reported in Fig. 2(b) for ^{64}Ni+^{58}Ni at 32 MeV/nucleon, where the positive sign indicates a net neutron flow from projectile to target leading to isospin equilibration, as expected. It is worth noting that $j_{\text{p.a.}}$ reaches its maximum value when the highest ρ/ρ_0 is reached by the system.

In order to build the weight function $w(\rho/\rho_0)$, we consider that the role of each explored density on the final phenomenon depends both on the amount of time spent by the system in that condition, and on the isospin current developing at the same time. Therefore, for a given impact parameter, a partial weight function is extracted by cumulating the baryonic density $\rho(t)/\rho_0$ over time, weighted by the corresponding $j_{\text{p.a.}}(t)$ as follows:

$$w_b(\rho/\rho_0) = \int_{t_{\text{start}}}^{t_{\text{stop}}} j_{\text{p.a.}}(t)\,\delta(\rho/\rho_0 - \rho(t)/\rho_0)\,dt \tag{7}$$

In this work, we integrate between $t_{\text{start}} = 0$ fm/c, corresponding to an initial distance between the projectile and target centers equal to 12 fm, and $t_{\text{stop}} = 80$ fm/c, when there is no further contribution of $j_{\text{p.a.}}$ (see Fig. 2(b)).

To take into account different impact parameters, since the different bs correspond to independent measurements, we take a simple sum of the partial weights:

$$w(\rho/\rho_0) = \sum_{b=b_{\text{min}}}^{b_{\text{max}}} w_b(\rho/\rho_0), \tag{8}$$

and consider the same $3 \le b(\text{fm}) \le 9$ interval as for the likelihood function.

4. Extracted symmetry energy constraint

Finally, our constraint for the symmetry energy behavior is shown by means of 1σ (yellow), 2σ (green), 3σ (blue) contours in Fig. 3. For comparison, the posterior distribution of $S(\rho/\rho_0)$ that would be obtained without the estimation of the density sensitive region (*i.e.* putting $w(\rho/\rho_0) = 1$) is shown as contours in the top-left inset of Fig. 3. Our results are in good agreement with the *ab initio* calculations from Refs. [25,42] but provide tighter constraints in the probed density region, pointing towards the softer side of the uncertainty band from χ-EFT plotted in gray. We stress that in this work, both the extraction of the symmetry energy confidence regions and of the baryonic densities probed via the study of isospin diffusion are treated in a consistent way within the same model framework. Interestingly, the fact that the sensitive region is close to saturation allows us to reject stiff behaviors like the one of the NL3 model, behaviors that are ruled out at high density [4], but could not have been discriminated with data probing only

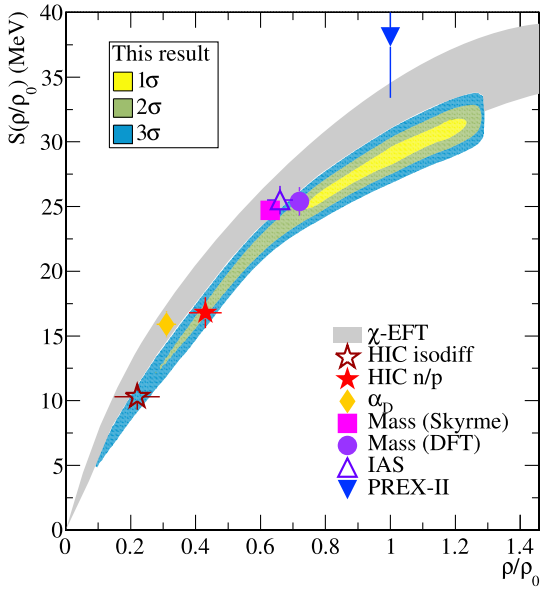

Fig. 3. Constraint on the density dependence of the symmetry energy obtained from this work, represented by the regions in yellow, green and blue corresponding to 1σ, 2σ, 3σ confidence levels respectively. The gray band indicates the microscopic uncertainty from [25]. Markers represent symmetry energy constraints available in the literature [43], extracted from isospin diffusion data in Sn+Sn HIC [44], from single and double ratios of n/p spectra [45], from analyses of nuclear masses [46,47], isobaric analog states [48] and electric dipole polarizability α_D [49], and from the neutron skin thickness of ^{208}Pb measured by PREX-II [50]. S confidence intervals for a set of ρ/ρ_0 values around the most sensitive region are reported in Table 1. (For interpretation of the references to colour in this figure legend, the reader is referred to the web version of this article.)

Table 1
Confidence intervals for the symmetry energy constraint presented in Fig. 3, for a set of ρ/ρ_0 values around the most sensitive region. The full result will be made available on HEP data.

ρ/ρ_0	S [MeV]	CI (1σ) [MeV]	CI (2σ) [MeV]	CI (3σ) [MeV]
0.75	25.09	[24.88,25.29]	[24.08,26.09]	[23.47,26.71]
0.80	25.93	[25.49,26.38]	[24.80,27.06]	[24.18,27.69]
0.85	26.73	[26.27,27.18]	[25.54,27.91]	[24.88,28.57]
0.90	27.49	[27.00,27.97]	[26.24,28.73]	[25.56,29.42]
0.95	28.20	[27.65,28.76]	[26.89,29.51]	[26.19,30.22]
1.00	28.87	[28.20,29.55]	[27.48,30.27]	[26.76,30.98]
1.05	29.51	[28.84,30.17]	[28.08,30.93]	[27.35,31.67]
1.10	30.10	[29.49,30.71]	[28.68,31.52]	[27.91,32.29]
1.15	30.65	[30.05,31.26]	[29.22,32.09]	[28.44,32.87]
1.20	31.17	[30.55,31.79]	[29.71,32.63]	[28.93,33.41]

densities below $\approx \rho_0/2$. The confidence regions we obtained slightly depend on the considered impact parameter interval: however, our main conclusions are stable against this arbitrary choice.

Fig. 3 also compares the result hereby presented with the constraints available in the literature [43]. We particularly note a remarkable agreement with previous results obtained from HIC, including isospin diffusion investigations in Sn+Sn systems [44], with the only difference lying in the declared density sensitivity interval.

5. Conclusions

In this work we have confronted the experimentally measured impact parameter dependence of the isospin transport ratio in ^{58,64}Ni+^{58,64}Ni collisions at 32 MeV/nucleon with the predictions of the BUU transport model using state-of-the-art effective nuclear energy density functionals that all respect the present constraints from *ab initio* calculations. A consistent study of the time dependence of the baryonic density and of the isospin current density allows a precise determination of the density region probed by the experiment. Our analysis is in good agreement with the *ab initio* predictions, and produces more stringent constraints on the density dependence of the symmetry energy term of the nuclear equation of state, with a posterior distribution which can be directly used for the inference of the EoS of astrophysical objects like neutron stars.

Data availability

The supporting experimental data for this article are from the e789_18 experiment and are registered as [51] following the GANIL Data Policy, and will be made available on request.
The complete final result will be made available on HEP Data.

Declaration of competing interest

The authors declare that they have no known competing financial interests or personal relationships that could have appeared to influence the work reported in this paper.

Acknowledgements

We acknowledge support from Région Normandie under Réseau d'Intérêt Normand FIDNEOS (RIN/FIDNEOS). This work was supported by the National Research Foundation of Korea (NRF), Grant No. 2018R1A5A1025563 and IBS-R031-D1. Many thanks are due to the accelerator staff of GANIL for delivering a very good quality beam and to the technical staff for the continuous support. S. Mallik acknowledges the GANIL Visiting Scientist program-2023 for very productive stay at Caen. S. Mallik also wishes to thank the VECC C&I Group for providing high-performance computational facilities.

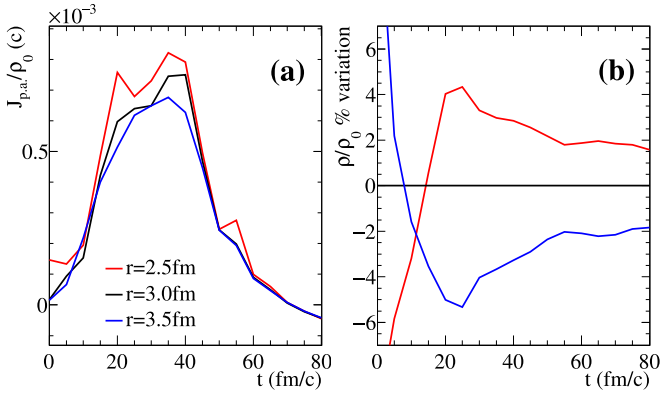

Fig. A.4. Time evolution of (a) the isospin current density along the principal axis $j_{\text{p.a.}}(t)$ for ^{64}Ni + ^{58}Ni at 32 MeV/nucleon, with $b = 5$ fm, for three different settings of the radius of the integration sphere $r = 2.5, 3.0, 3.5$ fm and (b) percentage variation of the baryonic density $\rho(t)$ with respect to the result for $r = 3.0$ fm adopted for our constraint.

Appendix A. Dependence of $\rho(t)$ and $j_{\text{p.a.}}(t)$ on the radius of the examination sphere

The time evolution of the baryonic density $\rho(t)$ and of the isospin current density along the principal axis $j_{\text{p.a.}}(t)$ shown in Fig. 2 needs an averaging of the local densities $\rho(\vec{r},t), j_{\text{p.a.}}(\vec{r},t)$ over a finite volume. In our work, an optimal value of 3 fm was found as the smallest radius ensuring a limited impact of the fluctuations. Fig. A.4 illustrates the effect of varying the radius by ± 0.5 fm around this optimal value on the extracted $\rho(t)$ and $j_{\text{p.a.}}(t)$ respectively: the corresponding percentage variation on the baryonic density is between 2 % and 5 %, except for the very first timesteps before the projectile-target contact.

In our analysis, this dependence of the baryonic and isospin current density on the examination sphere radius parameter r_0 is exclusively reflected in a corresponding modification of the weight function $w(\rho/\rho_0)$ applied to the likelihood function $\mathcal{L}(S(\rho/\rho_0))$. The maximum variation between the 1σ, 2σ, 3σ confidence levels resulting from the different radius r_0 settings is of the order of ± 3 % and concerns the highest densities explored by the contact region. We therefore conclude that our final constraint does not sensibly depend on the chosen setting for the radius of the integration sphere used for the $\rho(t)$ and $j_{\text{p.a.}}(t)$ extraction, and our result is hence stable against reasonable variations of such parameter.

References

[1] C. Ciampi, J.D. Frankland, D. Gruyer, N.L. Neindre, S. Mallik, R. Bougault, A. Chbihi, L. Baldesi, S. Barlini, E. Bonnet, B. Borderie, A. Camaiani, G. Casini, I. Dekhissi, D. Dell'aquila, J.A.D. Nas, Q. Fable, F. Gramegna, C. Gouyet, M. Henri, B. Hong, S. Kim, A. Kordyasz, T. Kozik, M.J. Kweon, I. Lombardo, O. Lopez, L. Manduci, T. Marchi, K. Mazurek, S.H. Nam, J. Park, M. Pârlog, G. Pasquali, S. Piantelli, G. Poggi, A. Rebillard-Soulié, R. Revenko, S. Valdré, G. Verde, E. Vient, Model-independent measurement of isospin diffusion in ni-ni systems at intermediate energy, Phys. Rev. C 111 (2025) 044601. https://doi.org/10.1103/PhysRevC.111.044601

[2] S. Huth, P.T.H. Pang, I. Tews, T. Dietrich, A.L. Fèvre, A. Schwenk, W. Trautmann, K. Agarwal, M. Bulla, M.W. Coughlin, C. Van Den Broeck , Constraining neutron-star matter with microscopic and macroscopic collisions, Nature 606 (2022) 276–280. https://www.nature.com/articles/s41586-022-04750-w.

[3] J.M. Lattimer, Neutron stars and the nuclear matter equation of state, Annu. Rev. Nuclear Particle Sci. 71 (2021) 433–464. https://doi.org/10.1146/annurev-nucl-102419-124827

[4] A. Sorensen, K. Agarwal, K.W. Brown, Z. Chajecki, P. Danielewicz, C. Drischler, S. Gandolfi, J.W. Holt, M. Kaminski, C.-M. Ko, R. Kumar, B.-A. Li, W.G. Lynch, A.B. Mcintosh, W.G. Newton, S. Pratt, O. Savchuk, M. Stefaniak, I. Tews, M.B. Tsang, R. Vogt, H. Wolter, H. Zbroszczyk, N. Abbasi, J. Aichelin, A. Andronic, S.A. Bass, F. Becattini, D. Blaschke, M. Bleicher, C. Blume, E. Bratkovskaya, B.A. Brown, D.A. Brown, A. Camaiani, G. Casini, K. Chatziioannou, A. Chbihi, M. Colonna, M.D. Cozma, V. Dexheimer, X. Dong, T. Dore, L. Du, J.A.D. nas, H. Elfner, W. Florkowski, Y. Fujimoto, R.J. Furnstahl, A. Gade, T. Galatyuk, C. Gale, F. Geurts, F. Gramegna, S. Grozdanov, K. Hagel, S.P. Harris, W. Haxton, U. Heinz, M.P. Heller, O. Hen, H. Hergert, N. Herrmann, H.Z. Huang, X.-G. Huang, N. Ikeno, G. Inghirami, J. Jankowski, J. Jia, J.C. Jiménez, J. Kapusta, B. Kardan, I. Karpenko, D. Keane, D. Kharzeev, A.

Kugler, A.L. Fèvre, D. Lee, H. Liu, M.A. Lisa, W.J. Llope, I. Lombardo, M. Lorenz, T. Marchi, L. Mclerran, U. Mosel, A. Motornenko, B. Müller, P. Napolitani, J.B. Natowitz, W. Nazarewicz, J. Noronha, J. Noronha-Hostler, G. Odyniec, P. Papakonstantinou, Z. Paulínyová, J. Piekarewicz, R.D. Pisarski, C. Plumberg, M. Prakash, J. Randrup, C. Ratti, P. Rau, S. Reddy, H.-R. Schmidt, P. Russotto, R. Ryblewski, A. Schäfer, B. Schenke, S. Sen, P. Senger, R. Seto, C. Shen, B. Sherrill, M. Singh, V. Skokov, M. Spaliński, J. Steinheimer, M. Stephanov, J. Stroth, C. Sturm, K.-J. Sun, A. Tang, G. Torrieri, W. Trautmann, G. Verde, V. Vovchenko, R. Wada, F. Wang, G. Wang, K. Werner, N. Xu, Z. Xu, H.-U. Yee, S. Yennello, Y. Yin, Dense nuclear matter equation of state from heavy-ion collisions, Prog. Part. Nucl. Phys., 134 (2024) 104080. https://www.sciencedirect.com/science/article/pii/S0146641023000613.

[5] H. Wolter, M. Colonna, D. Cozma, P. Danielewicz, C.M. Ko, R. Kumar, A. Ono, M.B. Tsang, J. Xu, Y.-X. Zhang, E. Bratkovskaya, Z.-Q. Feng, T. Gaitanos, A.L. Fèvre, N. Ikeno, Y. Kim, S. Mallik, P. Napolitani, D. Oliinychenko, T. Ogawa, M. Papa, J. Su, R. Wang, Y.-J. Wang, J. Weil, F.-S. Zhang, G.-Q. Zhang, Z. Zhang, J. Aichelin, W. Cassing, L.-W. Chen, H.-G. Cheng, H. Elfner, K. Gallmeister, C. Hartnack, S. Hashimoto, S. Jeon, K. Kim, M. Kim, B.-A. Li, C.-H. Lee, Q.-F. Li, Z.-X. Li, U. Mosel, Y. Nara, K. Niita, A. Ohnishi, T. Sato, T. Song, A. Sorensen, N. Wang, W.-J. Xie, Transport model comparison studies of intermediate-energy heavy-ion collisions, Prog. Part. Nucl. Phys. 125 (2022) 103962. https://www.sciencedirect.com/science/article/pii/S0146641022000230.

[6] J. Xu, H. Wolter, M. Colonna, M.D. Cozma, P. Danielewicz, C.M. Ko, A. Ono, M.B. Tsang, Y.-X. Zhang, H.-G. Cheng, N. Ikeno, R. Kumar, J. Su, H. Zheng, Z. Zhang, L.-W. Chen, Z.-Q. Feng, C. Hartnack, A.L. Fèvre, B.-A. Li, Y. Nara, A. Ohnishi, F.-S. Zhang, Comparing pion production in transport simulations of heavy-ion collisions at 270a MeV under controlled conditions, Phys. Rev. C 109 (2024) 044609. https://link.aps.org/doi/10.1103/PhysRevC.109.044609. https://doi.org/10.1103/PhysRevC.109.044609

[7] B.-A. Li, L.-W. Chen, C.M. Ko, Recent progress and new challenges in isospin physics with heavy-ion reactions, Phys. Rep. 464 (4) (2008) 113–281. https://www.sciencedirect.com/science/article/pii/S0370157308001269.

[8] J. Carlson, S. Gandolfi, F. Pederiva, S.C. Pieper, R. Schiavilla, K.E. Schmidt, R.B. Wiringa, Quantum monte carlo methods for nuclear physics, Rev. Mod. Phys. 87 (2015) 1067–1118. https://doi.org/10.1103/RevModPhys.87.1067

[9] D. Adhikari, H. Albataineh, D. Androic, K. Aniol, D.S. Armstrong, T. Averett, C. Gayoso, S. Barcus, V. Bellini, R.S. Beminiwattha, J.F. Benesch, H. Bhatt, D. Bhatta, D. Pathak, B. Bhetuwal, Q. Blaikie, A. Campagna, G.D. Camsonne, Y. Cates, C. Chen, J.C. Clarke, S. Cornejo, P.C. Dusa, A. Datta, D. Deshpande, C. Dutta, E. Feldman, C. Fuchey, D. Gal, T. Gaskell, M. Gautam, C. Gericke, I. Ghosh, J.-O. Halilovic, F. Hansen, W. Hauenstein, C.J. Henry, C. Horowitz, S. Jantzi, S. Jian, D.C. Johnston, B. Jones, S. Karki, C. Katugampola, P.M. Keppel, D.E. King, M. King, K.S. Knauss, T. Kumar, N. Kutz, G. Lashley-Colthirst, H. Leverick, N. Liu, S. Liyange, R. Malace, J. Mammei, M. Mammei, D. Mccaughan, D. Mcnulty, C. Meekins, R. Metts, M.M. Michaels, J. Mondal, A. Napolitano, D. Narayan, M.N.H. Nikolaev, V. Rashad, C. Owen, J. Palatchi, B. Pan, S. Pandey, K.D. Park, M. Paschke, M.L. Petrusky, S. Pitt, A.J.R. Premathilake, B. Puckett, R. Quinn, S. Radloff, A. Rahman, B.T. Rathnayake, P.E. Reed, R. Reimer, S. Richards, Y. Riordan, S. Roblin, A. Seeds, P. Shahinyan, L. Souder, M. Tang, Y. Thiel, G.M. Tian, E.W. Urciuoli, B. Wertz, B. Wojtsekhowski, T. Yale, A. Ye, A. Yoon, W. Zec, J. Zhang, X. Zhang, J. Zheng, Accurate determination of the neutron skin thickness of ^{208}Pb through parity-violation in electron scattering, Phys. Rev. Lett. 126 (2021) 172502. https://doi.org/10.1103/PhysRevLett.126.172502

[10] D. Adhikari, H. Albataineh, D. Androic, K.A. Aniol, D.S. Armstrong, T. Averett, C. Gayoso, S.K. Barcus, V. Bellini, R.S. Beminiwattha, J.F. Benesch, H. Bhatt, D. Bhatta, D. Bhatta Pathak, D. Bhetuwal, B. Blaikie, J. Boyd, Q. Campagna, A. Camsonne, G.D. Cates, Y. Chen, C. Clarke, J.C. Cornejo, S. Covrig Dusa, M.M. Dalton, P. Datta, A. Deshpande, D. Dutta, C. Feldman, E. Fuchey, C. Gal, D. Gaskell, T. Gautam, M. Gericke, C. Ghosh, I. Halilovic, J.-O. Hansen, O. Hassan, F. Hauenstein, W. Henry, C.J. Horowitz, C. Jantzi, S. Jian, S. Johnston, D.C. Jones, S. Kakkar, S. Katugampola, C. Keppel, P.M. King, D.E. King, K.S. Kumar, T. Kutz, N. Lashley-Colthirst, G. Leverick, H. Liu, N. Liyanage, J. Mammei, R. Mammei, M. Mccaughan, D. Mcnulty, D. Meekins, C. Metts, R. Michaels, M. Mihovilovic, M. Mondal, J. Napolitano, A. Narayan, D. Nikolaev, V. Owen, C. Palatchi, J. Pan, B. Pandey, S. Park, K.D. Paschke, M. Petrusky, M.L. Pitt, S. Premathilake, B. Quinn, R. Radloff, R. Rahman, M.N.H. Rashad, A. Rathnayake, B.T. Reed, P.E. Reimer, R. Richards, S. Riordan, Y.R. Roblin, S. Seeds, A. Shahinyan, P. Souder, M. Thiel, Y. Tian, G.M. Urciuoli, E.W. Wertz, B. Wojtsekhowski, B. Yale, T. Ye, A. Yoon, W. Xiong, A. Zec, W. Zhang, J. Zhang, X. Zheng, Precision determination of the neutral weak form factor of ^{48}Ca, Phys. Rev. Lett. 129 (2022) 042501. https://doi.org/10.1103/PhysRevLett.129.042501

[11] B.P. Abbott, R. Abbott, T.D. Abbott, F. Acernese, K. Ackley, C. Adams, T. Adams, P. Addesso, R.X. Adhikari, V.B. Adya, C. Affeldt, B. Agarwal, M. Agathos, K. Agatsuma, N. Aggarwal, O.D. Aguiar, L. Aiello, A. Ain, P. Ajith, B. Allen, G. Allen, A. Allocca, M.A. Aloy, P.A. Altin, A. Amato, A. Ananyeva, S.B. Anderson, W.G. Anderson, S.V. Angelova, S. Antier, S. Appert, K. Arai, M.C. Araya, J.S. Areeda, Properties of the binary neutron star merger gw170817, Phys. Rev. X 9 (2019) 11001. https://doi.org/10.1103/PhysRevX.9.011001

[12] F. Rami, Y. Leifels, B.D. Schauenburg, A. Gobbi, B. Hong, J.P. Alard, A. Andronic, R. Averbeck, V. Barret, Z. Basrak, N. Bastid, I. Belyaev, A. Bendarag, G. Berek, R. Čaplar, N. Cindro, P. Crochet, A. Devismes, P. Dupieux, M. Dželalija, M. Eskef, C. Finck, Z. Fodor, H. Folger, L. Fraysse, A. Genoux-Lubain, Y. Grigorian, Y. Grishkin, N. Herrmann, K.D. Hildenbrand, J. Kecskemeti, Y.J. Kim, P. Koczon, M. Kirejczyk, M. Korolija, R. Kotte, M. Kowalczyk, T. Kress, R. Kutsche, A. Lebedev, K.S. Lee, V. Manko, H. Merlitz, S. Mohren, D. Moisa, J. Mösner, W. Neubert, A. Nianine, D. Pelte, M. Petrovici, C. Pinkenburg, C. Plettner, W. Reisdorf, J. Ritman, D. Schüll, Z. Seres, B. Sikora, K.S. Sim, V. Simion, K. Siwek-Wilczyńska, A. Somov, M.R. Stockmeier, G. Stoicea, M. Vasiliev, P. Wagner, K. Wiśniewski, D. Wohlfarth, J.T. Yang, I. Yushmanov, A. Zhilin, Isospin tracing: a probe of nonequilibrium in central heavy-ion collisions, Phys. Rev. Lett. 84 (2000) 1120–1123. https://doi.org/10.1103/PhysRevLett.84.1120

[13] M.B. Tsang, W.A. Friedman, C.K. Gelbke, W.G. Lynch, G. Verde, H.S. Xu, Isotopic scaling in nuclear reactions, Phys. Rev. Lett. 86 (2001) 5023–5026. https://doi.org/10.1103/PhysRevLett.86.5023

[14] M.B. Tsang, J.R. Stone, F. Camera, P. Danielewicz, S. Gandolfi, K. Hebeler, C.J. Horowitz, J. Lee, W.G. Lynch, Z. Kohley, R. Lemmon, P. Möller, T. Murakami, S. Riordan, X. Roca-Maza, F. Sammarruca, A.W. Steiner, I.V. na, S.J. Yennello, Constraints on the symmetry energy and neutron skins from experiments and theory, Phys. Rev. C 86 (2012) 15803. https://doi.org/10.1103/PhysRevC.86.015803

[15] Y. Zhang, D.D.S. Coupland, P. Danielewicz, Z. Li, H. Liu, F. Lu, W.G. Lynch, M.B. Tsang, Influence of in-medium nn cross sections, symmetry potential, and impact parameter on isospin observables, Phys. Rev. C 85 (2012) 24602. https://doi.org/10.1103/PhysRevC.85.024602

[16] B.-A. Li, X. Han, Constraining the neutron-proton effective mass splitting using empirical constraints on the density dependence of nuclear symmetry energy around normal density, Phys. Lett. B 727 (1) (2013) 276–281. https://www.sciencedirect.com/science/article/pii/S0370269313007995.

[17] M. Oertel, M. Hempel, T. Klähn, S. Typel, Equations of state for supernovae and compact stars, Rev. Mod. Phys. 89 (1) (2017) 15007.

[18] B.-A. Li, B.-J. Cai, W.-J. Xie, N.-B. Zhang, Progress in constraining nuclear symmetry energy using neutron star observables since gw170817, 7, 2021. https://www.mdpi.com/2218-1997/7/6/182.

[19] C. Ciampi, S. Piantelli, G. Casini, G. Pasquali, J. Quicray, L. Baldesi, S. Barlini, B. Borderie, R. Bougault, A. Camaiani, A. Chbihi, D. Dell'aquila, M. Cicerchia, J.A.D. nas, Q. Fable, D. Fabris, J.D. Frankland, C. Frosin, T. Génard, F. Gramegna, D. Gruyer, M. Henri, B. Hong, S. Kim, A. Kordyasz, T. Kozik, M.J. Kweon, J. Lemarié, N.L. Neindre, I. Lombardo, O. Lopez, T. Marchi, S.H. Nam, A. Ordine, P. Ottanelli, J. Park, J.H. Park, M. Pârlog, G. Poggi, A. Rebillard-Soulié, A.A. Stefanini, S. Upadhyaya, S. Valdré, G. Verde, E. Vient, M. Vigilante, First results from the INDRA-FAZIA apparatus on isospin diffusion in 58,64Ni 58,64Ni systems at Fermi energies, Phys. Rev. C 106 (2) (2022) 024603. https://doi.org/10.1103/PhysRevC.106.024603

[20] S. Mallik, F. Gulminelli, D. Gruyer, Constraining the density dependence of the symmetry energy: the isospin transport ratio revisited, J. Phys. G Nucl. Part. Phys. 49 (1) (2021) 15102. https://doi.org/10.1088/1361-6471/ac3473

[21] A. Camaiani, S. Piantelli, A. Ono, G. Casini, B. Borderie, R. Bougault, C. Ciampi, J.A.D. nas, C. Frosin, J.D. Frankland, D. Gruyer, N. Leneindre, I. Lombardo, G. Mantovani, P. Ottanelli, M. Parlog, G. Pasquali, S. Upadhyaya, S. Valdré, G. Verde, E. Vient, Influence of fast emissions and statistical de-excitation on the isospin transport ratio, Phys. Rev. C 102 (4) (2020) 44607. https://doi.org/10.1103/PhysRevC.102.044607

[22] R. Bougault, G. Poggi, S. Barlini, B. Borderie, G. Casini, A. Chbihi, N.L. Neindre, M. Pârlog, G. Pasquali, S. Piantelli, Z. Sosin, G. Ademard, R. Alba, A. Anastasio, S. Barbey, L. Bardelli, M. Bini, A. Boiano, M. Boisjoli, E. Bonnet, R. Borcea, B. Bougard, G. Brulin, M. Bruno, S. Carboni, C. Cassese, F. Cassese, M. Cinausero, L. Ciolacu, I. Cruceru, M. Cruceru, B. Aquino, B.D. Fazio, M. Degerlier, P. Desrues, P.D. Meo, J.A.D. Nas, P. Edelbruck, S. Energico, M. Falorsi, J.D. Frankland, E. Galichet, K. Gasior, F. Gramegna, R. Giordano, D. Gruyer, A. Grzeszczuk, M. Guerzoni, H. Hamrita, C. Huss, M. Kajetanowicz, K. Korcyl, A. Kordyasz, T. Kozik, P. Kulig, L. Lavergne, E. Legouée, O. Lopez, J.L. ukasik, C. Maiolino, T. Marchi, P. Marini, I. Martel, V. Masone, A. Meoli, Y. Merrer, L. Morelli, F. Negoita, A. Olmi, A. Ordine, G. Paduano, C. Pain, M.P. ka, G. Passeggio, G. Pastore, P.P. owski, M. Petcu, H. Petrascu, E. Piasecki, G. Pontoriere, E. Rauly, M.F. Rivet, R. Rocco, E. Rosato, L. Roscilli, E. Scarlini, F. Salomon, D. Santonocito, V. Seredov, S. Serra, D. Sierpowski, G. Spadaccini, C. Spitaels, A.A. Stefanini, G. Tobia, G. Tortone, T. Twaróg, S. Valdré, A. Vanzanella, E. Vanzanella, E. Vient, M. Vigilante, G. Vitiello, E. Wanlin, A. Wieloch, W. Zipper, The fazia project in europe: R&d phase, Eur. Phys. J. A 50 (2014) 47. https://doi.org/10.1140/epja/i2014-14047-4

[23] S. Valdré, G. Casini, N.L. Neindre, M. Bini, A. Boiano, B. Borderie, P. Edelbruck, G. Poggi, F. Salomon, G. Tortone, R. Alba, S. Barlini, E. Bonnet, B. Bougard, R. Bougault, G. Brulin, M. Bruno, A. Buccola, A. Camaiani, A. Chbihi, C. Ciampi, M. Cicerchia, M. Cinausero, D. Dell'aquila, P. Desrues, J.D. nas, D. Fabris, M. Falorsi, J. Frankland, C. Frosin, E. Galichet, R. Giordano, F. Gramegna, L. Grassi, D. Gruyer, M. Guerzoni, M. Henri, M. Kajetanowicz, K. Korcyl, A. Kordyasz, T. Kozik, P. Lecomte, I. Lombardo, O. Lopez, C. Maiolino, G. Mantovani, T. Marchi, A. Margotti, Y. Merrer, L. Morelli, A. Olmi, A. Ordine, P. Ottanelli, C. Pain, M.P. ka, M. Pârlog, G. Pasquali, G. Pastore, S. Piantelli, H.D. Préaumont, R. Revenko, A. Richard, M. Rivet, J. Ropert, E. Rosato, F. Saillant, D. Santonocito, E. Scarlini, S. Serra, C. Soulet, G. Spadaccini, A. Stefanini, G. Tobia, S. Upadhyaya, A. Vanzanella, G. Verde, E. Vient, M. Vigilante, E. Wanlin, G. Wittwer, A. Zucchini, The FAZIA setup: a review on the electronics and the mechanical mounting, Nucl. Instrum. Methods Phys. Res. Sect. A 930 (2019) 27–36. https://linkinghub.elsevier.com/retrieve/pii/S0168900219304243.

[24] J.D. Frankland, D. Gruyer, E. Bonnet, B. Borderie, R. Bougault, A. Chbihi, J.E. Ducret, D. Durand, Q. Fable, M. Henri, J. Lemarié, N.L. Neindre, I. Lombardo, O. Lopez, L. Manduci, M. Pârlog, J. Quicray, G. Verde, E. Vient, M. Vigilante, Model independent reconstruction of impact parameter distributions for intermediate energy heavy ion collisions, Phys. Rev. C 104 (2021) 034609. https://doi.org/10.1103/PhysRevC.104.034609

[25] C. Drischler, K. Hebeler, A. Schwenk, Asymmetric nuclear matter based on chiral two- and three-nucleon interactions, Phys. Rev. C 93 (2016) 54314. https://doi.org/10.1103/PhysRevC.93.054314

[26] V. Baran, M. Colonna, V. Greco, M.D. Toro, Reaction dynamics with exotic nuclei, Phys. Rep. 410 (5) (2005) 335–466. https://www.sciencedirect.com/science/article/pii/S0370157305000025.

[27] C. Ciampi, S. Piantelli, G. Casini, A. Ono, J.D. Frankland, L. Baldesi, S. Barlini, B. Borderie, R. Bougault, A. Camaiani, A. Chbihi, J.A.D. nas, Q. Fable, D. Fab-

ris, C. Frosin, T. Génard, F. Gramegna, D. Gruyer, M. Henri, B. Hong, S. Kim, A. Kordyasz, T. Kozik, M.J. Kweon, N.L. Neindre, I. Lombardo, O. Lopez, T. Marchi, K. Mazurek, S.H. Nam, J. Park, M. Pârlog, G. Pasquali, G. Poggi, A. Rebillard-Soulié, A.A. Stefanini, S. Upadhyaya, S. Valdré, G. Verde, E. Vient, M. Vigilante, Quasiprojectile breakup and isospin equilibration at Fermi energies: potential indication of longer projectile-target contact times, Phys. Rev. C 108 (5) (2023) 054611. https://doi.org/10.1103/PhysRevC.108.054611

[28] S. Mallik, S.D. Gupta, G. Chaudhuri, Event simulations in a transport model for intermediate energy heavy ion collisions: applications to multiplicity distributions, Phys. Rev. C 91 (2015) 34616. https://doi.org/10.1103/PhysRevC.91.034616

[29] S. Mallik, G. Chaudhuri, Isospin dependent hybrid model for studying isoscaling in heavy ion collisions around the fermi energy domain, Nucl. Phys. A 1002 (2020) 121948. https://www.sciencedirect.com/science/article/pii/S037594742030258X.

[30] M. Colonna, Y.-X. Zhang, Y.-J. Wang, D. Cozma, P. Danielewicz, C.M. Ko, A. Ono, M.B. Tsang, R. Wang, H. Wolter, J. Xu, Z. Zhang, L.-W. Chen, H.-G. Cheng, H. Elfner, Z.-Q. Feng, M. Kim, Y. Kim, S. Jeon, C.-H. Lee, B.-A. Li, Q.-F. Li, Z.-X. Li, S. Mallik, D. Oliinychenko, J. Su, T. Song, A. Sorensen, F.-S. Zhang, Comparison of heavy-ion transport simulations: mean-field dynamics in a box, Phys. Rev. C 104 (2021) 024603. https://doi.org/10.1103/PhysRevC.104.024603

[31] Y.-X. Zhang, Y.-J. Wang, M. Colonna, P. Danielewicz, A. Ono, M.B. Tsang, H. Wolter, J. Xu, L.-W. Chen, D. Cozma, Z.-Q. Feng, S.D. Gupta, N. Ikeno, C.-M. Ko, B.-A. Li, Q.-F. Li, Z.-X. Li, S. Mallik, Y. Nara, T. Ogawa, A. Ohnishi, D. Oliinychenko, M. Papa, H. Petersen, J. Su, T. Song, J. Weil, N. Wang, F.-S. Zhang, Z. Zhang, Comparison of heavy-ion transport simulations: collision integral in a box, Phys. Rev. C 97 (2018) 34625. https://doi.org/10.1103/PhysRevC.97.034625

[32] S.J. Lee, H.H. Gan, E.D. Cooper, S.D. Gupta, Nuclei with diffuse surfaces for future boltzmann-uehling-uhlenbeck calculations, Phys. Rev. C 40 (1989) 2585–2591. https://doi.org/10.1103/PhysRevC.40.2585

[33] W.D. Myers, A model for high-energy heavy-ion collisions, Nucl. Phys. A 296 (1) (1978) 177–188. https://www.sciencedirect.com/science/article/pii/0375947478904207.

[34] J. Margueron, R.H. Casali, F. Gulminelli, Equation of state for dense nucleonic matter from metamodeling. i. foundational aspects, Phys. Rev. C 97 (2018) 25805. https://doi.org/10.1103/PhysRevC.97.025805

[35] G.A. Lalazissis, J. König, P. Ring, New parametrization for the lagrangian density of relativistic mean field theory, Phys. Rev. C 55 (1997) 540–543. https://doi.org/10.1103/PhysRevC.55.540

[36] N.V. Giai, H. Sagawa, Spin-isospin and pairing properties of modified skyrme interactions, Phys. Lett. B 106 (5) (1981) 379–382. https://www.sciencedirect.com/science/article/pii/0370269381906468.

[37] B.T. Reed, F.J. Fattoyev, C.J. Horowitz, J. Piekarewicz, Density dependence of the symmetry energy in the post-prex-crex era, Phys. Rev. C 109 (2024) 035803. https://doi.org/10.1103/PhysRevC.109.035803

[38] Z. Xiao, B.-A. Li, L.-W. Chen, G.-C. Yong, M. Zhang, Circumstantial evidence for a soft nuclear symmetry energy at suprasaturation densities, Phys. Rev. Lett. 102 (2009) 62502. https://doi.org/10.1103/PhysRevLett.102.062502

[39] X. Roca-Maza, G. Colò, H. Sagawa, New skyrme interaction with improved spin-isospin properties, Phys. Rev. C 86 (2012) 31306. https://doi.org/10.1103/PhysRevC.86.031306

[40] R.J. Lenk, V.R. Pandharipande, Nuclear mean field dynamics in the lattice hamiltonian vlasov method, Phys. Rev. C 39 (1989) 2242–2249. https://doi.org/10.1103/PhysRevC.39.2242

[41] S. Mallik, G. Chaudhuri, F. Gulminelli, Sensitivity of the evaporation residue observables to the symmetry energy, Phys. Rev. C 100 (2019) 24611. https://doi.org/10.1103/PhysRevC.100.024611

[42] S. Huth, C. Wellenhofer, A. Schwenk, New equations of state constrained by nuclear physics, observations, and qcd calculations of high-density nuclear matter, Phys. Rev. C 103 (2021) 025803. https://doi.org/10.1103/PhysRevC.103.025803

[43] W. Lynch, M. Tsang, Decoding the density dependence of the nuclear symmetry energy, Phys. Lett. B 830 (2022) 137098. https://www.sciencedirect.com/science/article/pii/S0370269322002325.

[44] M.B. Tsang, Y. Zhang, P. Danielewicz, M. Famiano, Z. Li, W.G. Lynch, A.W. Steiner, Constraints on the density dependence of the symmetry energy, Phys. Rev. Lett. 102 (2009) 122701. https://doi.org/10.1103/PhysRevLett.102.122701

[45] P. Morfouace, C. Tsang, Y. Zhang, W. Lynch, M. Tsang, D. Coupland, M. Youngs, Z. Chajecki, M. Famiano, T. Ghosh, G. Jhang, J. Lee, H. Liu, A. Sanetullaev, R. Showalter, J. Winkelbauer, Constraining the symmetry energy with heavy-ion collisions and bayesian analyses, Phys. Lett. B 799 (2019) 135045. https://www.sciencedirect.com/science/article/pii/S0370269319307671.

[46] B.A. Brown, Constraints on the skyrme equations of state from properties of doubly magic nuclei, Phys. Rev. Lett. 111 (2013) 232502. https://doi.org/10.1103/PhysRevLett.111.232502

[47] M. Kortelainen, J. Mcdonnell, W. Nazarewicz, P.-G. Reinhard, J. Sarich, N. Schunck, M.V. Stoitsov, S.M. Wild, Nuclear energy density optimization: large deformations, Phys. Rev. C 85 (2012) 24304. https://doi.org/10.1103/PhysRevC.85.024304

[48] P. Danielewicz, J. Lee, Symmetry energy ii: isobaric analog states, Nucl. Phys. A 922 (2014) 1–70. https://www.sciencedirect.com/science/article/pii/S0375947413007872.

[49] Z. Zhang, L.-W. Chen, Electric dipole polarizability in ^{208}Pb as a probe of the symmetry energy and neutron matter around $\rho\_0/3$, Phys. Rev. C 92 (2015) 31301. https://doi.org/10.1103/PhysRevC.92.031301

[50] B.T. Reed, F.J. Fattoyev, C.J. Horowitz, J. Piekarewicz, Implications of prex-2 on the equation of state of neutron-rich matter, Phys. Rev. Lett. 126 (2021) 172503. https://doi.org/10.1103/PhysRevLett.126.172503

[51] E789_18 GANIL dataset, 2019. https://doi.org/10.26143/ganil-2019-e789_18